# Chapter-3

## Biomimetic self-assembly of colloidal ZnO nanoclusters via Oriented attachment crystal growth.

## 3.1 Synthesis methodology

The synthesis of self-assembled, preferentially aligned ZnO nanoclusters was carried out through modified sol gel process. Zinc acetate dihydrate, ethanol and diethanolamine were used as metal oxide precursor, solvent and complexing agent respectively. Sodium hydroxide was used as a source of hydroxyl ions to maintain optimum pH during the course of the reaction.

Initially, 50 ml of ethanol was heated to 60ºC in a round bottomed flask equipped with a magnetic stirrer. Then, 550 mg of $Zn(CH_3COO)_2.2H_2O$ was added to prepare a 0.05 M solution which was heated to reflux at 80ºC for another hour. Diethanolamine (240 microliter) with DEA: $Zn^{2+}$ molar ratio of 1:1 was added dropwise to the solution with intense magnetic stirring. After sufficient mixing 0.2 M NaOH Ethanol solution, with Na: $Zn^{2+}$ molar ratio of 1:1 was slowly added dropwise and the complex mixture was allowed to reflux for another 2 hours. The resulting transparent, homogenous sol was aged overnight and cooled to room temperature. Owing to the high stability of the prepared sol, no precipitates were visible. Surface capping of the nucleated nanocrystals at an early growth stage and presence of an optimum amount of hydroxyl ions limited the formation of $Zn(OH)_2$ and other zinc-oxo complexes resulting in a stable, transparent sol consisting of monodisperse ZnO mesocrystals. The solution was centrifuged twice for 20 min at 5000 rpm to break down agglomerates and separate bigger sized particles if any. The supernatant was filtered through a micron-sized membrane to remove impurities or unreacted salts. The purified sol was stored under ambient conditions in air-tight glass scintillation vials for further characterization.

## 3.2 Oriented Attachment (OA) growth process

Since its first description in 1900, Ostwald Ripening [150] has been considered the most accepted mechanism of crystal growth where the high surface energy of smaller nuclei controls their dissolution in the precursor solution to pave way for bigger nuclei to grow even more. Although, the recent studies on crystal growth in bio-minerals and other nano engineered structures such as nanowires have shed light on a completely different process of nanoparticle growth, through agglomeration and coalignment of nuclei, that challenges the classical

nucleation and growth models. The resulting crystals often exhibit complex forms ranging from quasi–one-dimensional (1D) chains to 3D hierarchical and self-similar nanoclusters. [151]

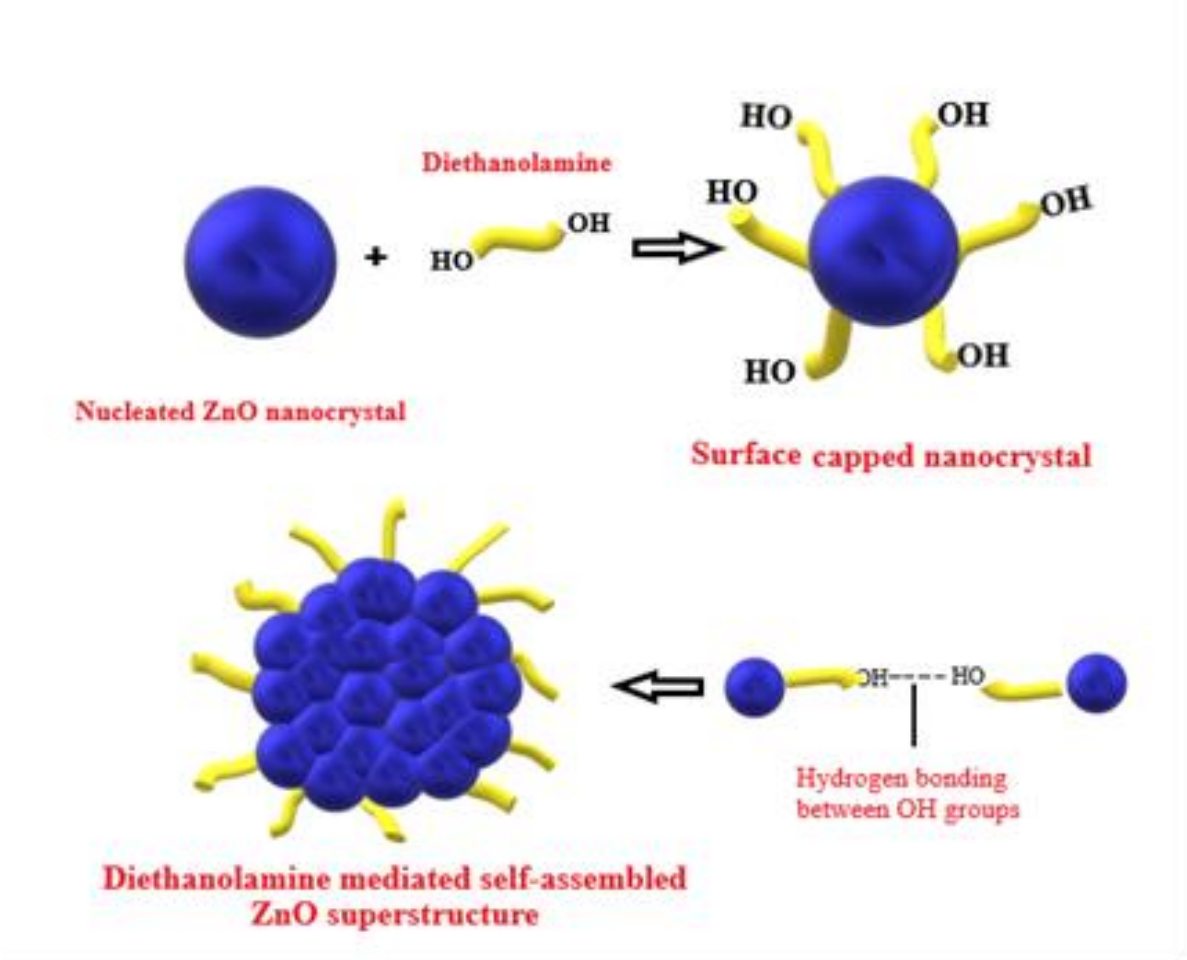


Fig 3.1- Schematic description of ZnO nanocrystal surface modification and diethanolamine assisted self-assembly into ordered nanoclusters.

Li et al in a recent study monitored the Oriented attachment growth in iron oxide nanoparticles via in situ HR-TEM and made some significant conclusions regarding the dynamics of alignment and attachment processes.[151] The study revealed that the particles continuously diffused and rotated, repeatedly contacting one another until attachment finally occurred. Following the attachment, the space between the particles was filled on the order of 10 to 100 s. To make this contact the particles were seen to ’jump’ in the range of 0.5−1 nm, and it has been suggested that this attraction is coulombic in nature. However, van der Waals’s interactions with anisotropic polarizability cannot be ruled out. [152]

In our work, we nano-engineered anisotropic ZnO mesocrystals that obeyed a similar Oriented attachment crystal growth. Fig 3.1 depicts the ligand mediated self-assembly of ZnO nanoclusters. Diethanolamine molecules bind with the negatively charged ZnO surface through ionic dipolar interactions between the oxygen atom from ZnO and hydrogen atom from OH group of surfactant. Next, the surface capped ZnO nanocrystals obey coalignment and coalescence process mediated via hydrogen bonding forces resulting in highly ordered nanoclusters with aligned crystal lattices. Such lattice aligned ZnO nanoclusters with a high degree of preferential orientation along a-axis and nanocrystallite size in the quantum regime have not been synthesized before through diethanolamine mediated facile sol gel synthesis. Fig 3.2 depicts high resolution TEM image of a self-assembled nanostructure with individual crystallites ranging between 3-5 nm. Neighbouring nanocrystals exhibit a high degree of lattice alignment between their respective crystal planes. Also, the orientation of crystal planes appears homogenous throughout the nanostructure suggesting an efficient Oriented attachment mechanism with a preferential growth direction.

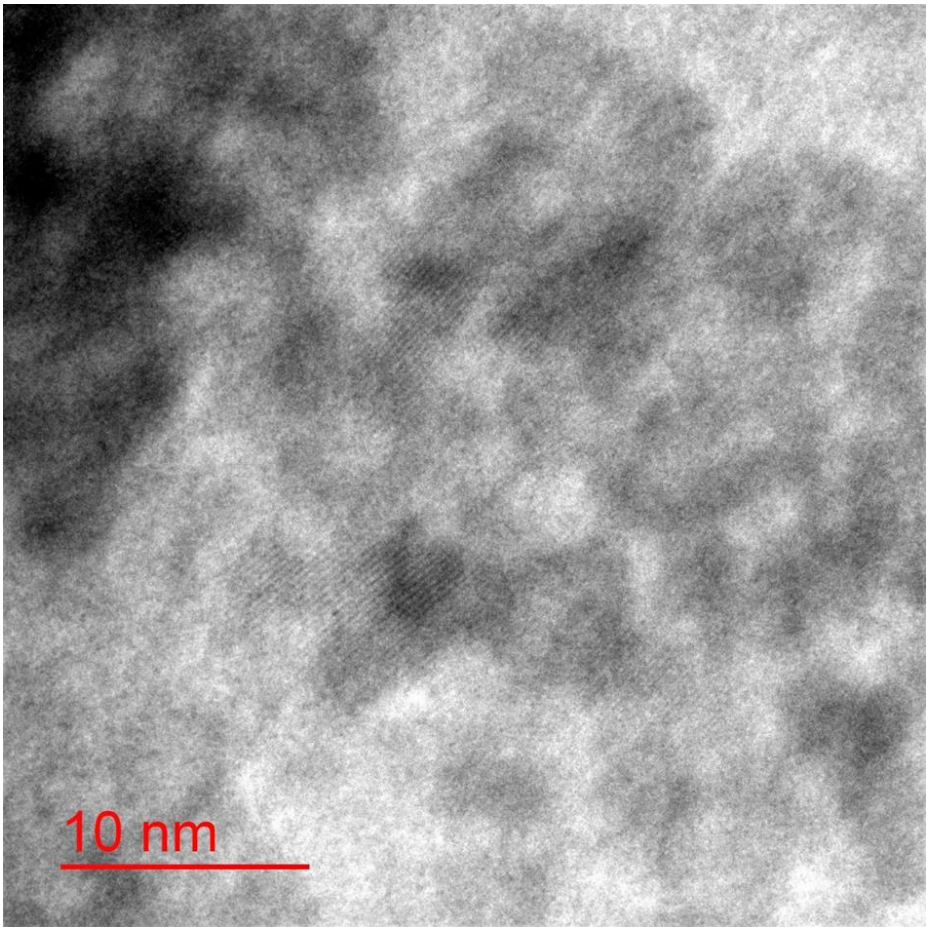

Fig 3.2- HR-TEM image of a single ZnO superstructure illuminating oriented attachment of crystal planes between neighboring Quantum dots.

## 3.3 Experimental methods

**XRD-** Crystallographic studies of ZnO mesocrystals was carried out on Rigaku Miniflex-600 equipped with Cu-Kα radiation and graphite monochromator.

**HRTEM-** Size of nanoclusters and nano-crystallites, morphology, crystal growth mechanism and lattice orientation were studied using a Tecnai G2 20 Twin High resolution Transverse Electron Microscope by FEI USA. Colloidal ZnO dispersion was drop cast on a carbon-coated copper grid and was dried in a vacuum oven at 60ºC for one hour before analysis.

**DLS, ZETA-** Polydispersity index, surface potential and long term colloidal stability of highly dilute ZnO ethanol suspension was acquired at 25ºC equilibrium temperature using Zetasizer Nano ZS system by Malvern Panalytical.

**UV-Vis Spectroscopy-** The UV-Vis absorption spectra was recorded on dilute ZnO ethanol suspension with pure ethanol as reference using BioSpectrometer kinetic by Eppendorf and was used to calculate the band gap energy and size of quantum dots.

**PLE-** Photoluminescence emission spectra of ZnO nanoclusters and ZnO/PMMA hybrids was acquired in the wavelength range 400-800 nm using Fluorescence Spectrophotometer F-4600 by Hitachi with excitation and emission slit width 10 nm and PMT voltage 700 V.

## 3.4 Results & Discussion

### 3.4.1 Morphology and Self-assembly

TEM images (Fig 3.3) illuminated the uniform size distribution and homogenous dispersion of ZnO nanostructures with an avg. size of 50 nm. Further close inspection indicated that the observed nanostructures didn't possess the usual bulk morphology rather these nanoclusters were composed of self-assembled quantum dots, with individual sizes in the quantum regime (3-5 nm), resulting in a porous texture with increased effective surface area. These nanoclusters with enhanced surface area could significantly improve the photocatalytic and sensing

properties of hybrid thin films owing to the increase in absorption cross section and large number of surface defects. Histograms of nanocluster size distribution and quantum dot size distribution within a nanocluster were plotted using ImageJ software for HRTEM image analysis (Fig 3.4). The plots indicate a uniform size distribution with maximum number of particles in the range of 40-50 nm. The nanocrystallite size distribution confirms that all the individual crystallites had sizes in the quantum regime with a peak around 4.5 nm.

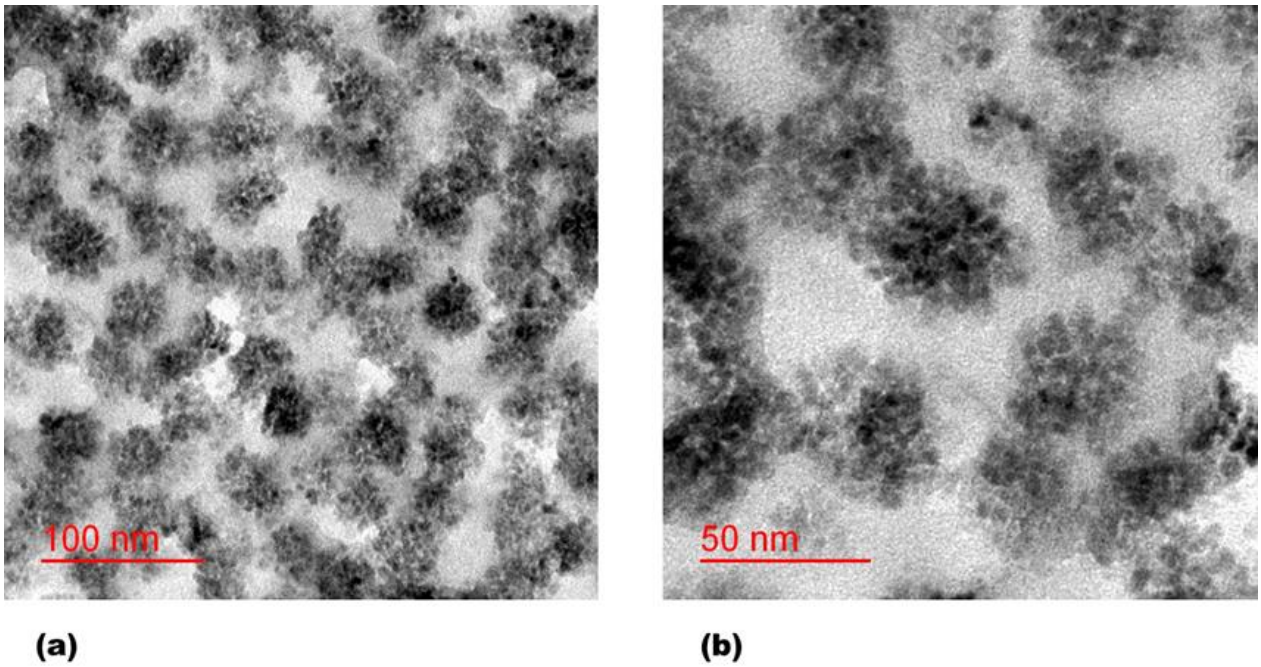


Fig 3.3- TEM images of ZnO nanoclusters illuminating (a) Uniform and homogenous distribution of self-assembled structures at 100 nm resolution, (b) Porous morphology with individual QD's in 3-5 nm range at 50 nm resolution.

TEM was employed in high resolution mode to study the orientation and interplanar spacing of crystal planes. (Fig 3.5 a, b) Oriented attachment process was quite evident in the HRTEM images since the crystal planes of adjacent nanocrystals were aligned in the final nanocluster. The preferred orientation of crystal growth was also confirmed as maximum nanocrystals had planes aligned in the same direction. The d-spacing measured between two such planes was 0.28 nm which is the standard value of spacing for a <100> plane. Hence it was established that the nanostructures crystallized with a preferred orientation along the a-axis. This is in excellent agreement with the XRD data where we observed a very sharp and intense <100> peak and other major peaks were absent from the spectra. The imaging was performed in diffraction mode to extract information about the crystal structure. The formation of rings indicated the material is polycrystalline in nature. The most prominent ring with high intensity

corresponded to <100> plane as expected, owing to the preferential growth direction and the intensity diminished sharply for all other planes.

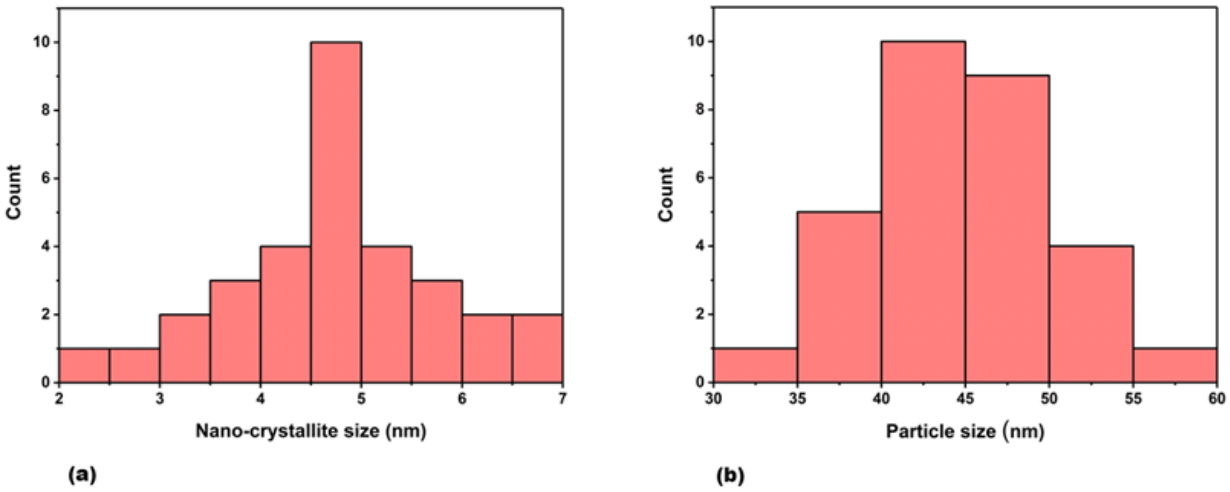


Fig 3.4- Histograms of (a) Size distribution of Quantum dots constituting a single nanocluster and (b) Size distribution of ZnO nanoclusters in the colloidal suspension.

EDAX spectrum confirmed the elemental composition of nanoclusters with prominent Zn-Kα, Kβ, Zn-L, O-K peaks. N-K due to its extremely small concentration did not show a recognizable peak while the carbon and copper peaks arose from the TEM grid. EDAX spectra also confirmed the absence of any undesirable impurity elements.

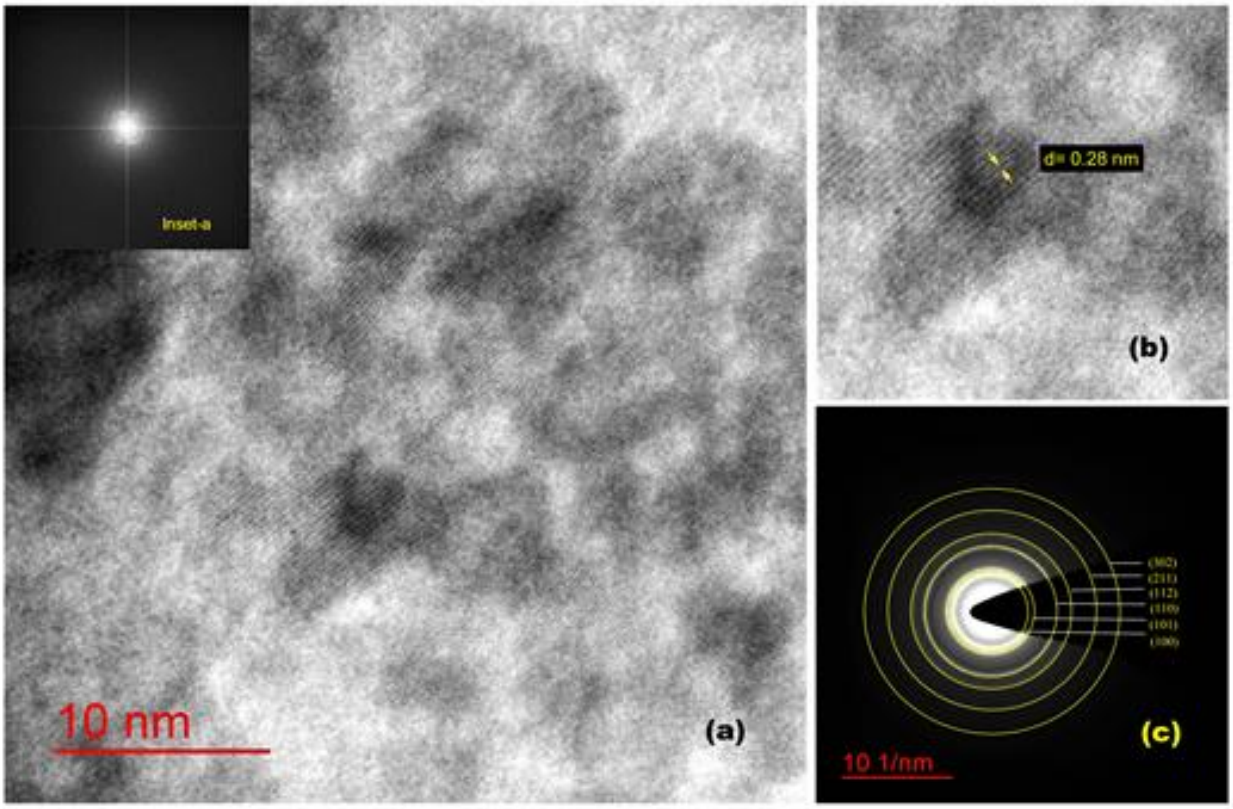


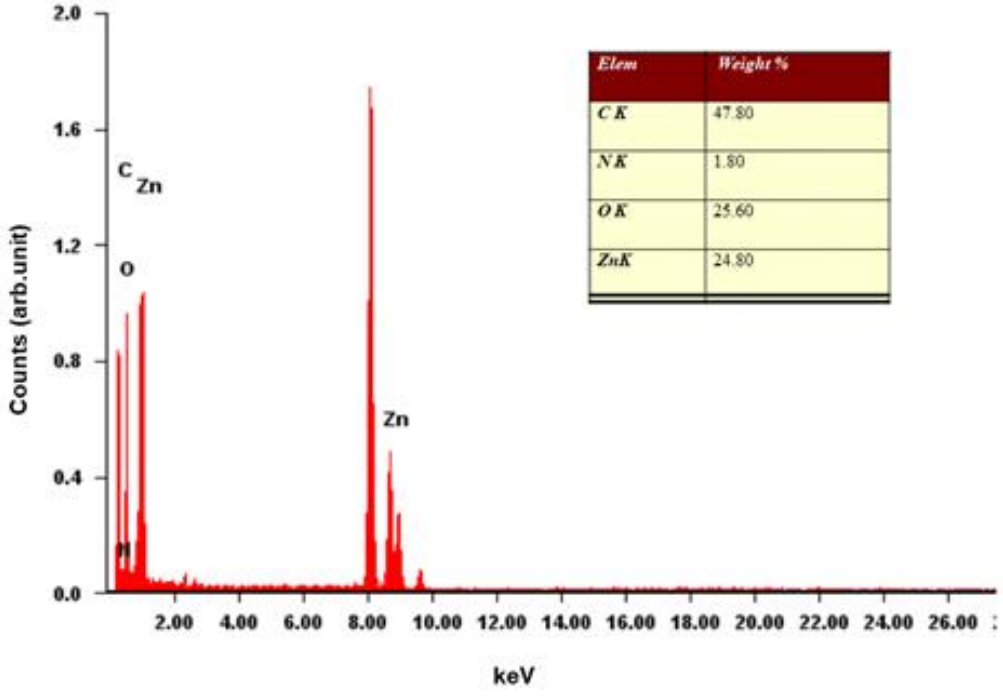


| Elem | Weight % |
|---|---|
| C K | 47.80 |
| N K | 1.80 |
| O K | 25.60 |
| Zn K | 24.80 |

Fig 3.5- Top panel: (a) HRTEM image depicting highly aligned adjacent crystal planes with inset-a Fast Fourier transform of lattice planes, (b) Interplanar spacing of a nano-crystallite corresponding to <100> plane and (c) SAED pattern in reciprocal space.

Bottom panel: EDAX spectra of ZnO nanoclusters, inset- weight % of constituent elements

## 3.4.2 Crystallographic studies

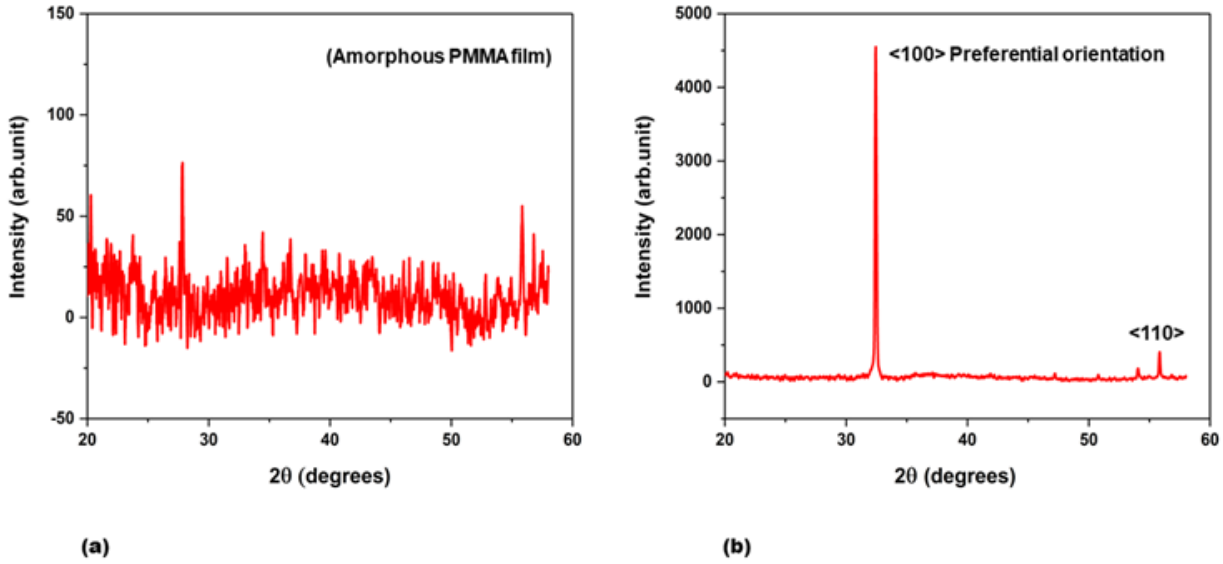


Fig 3.6- X-ray diffraction patterns of (a) Pure PMMA thin film and (b) 0.5 wt % PMMA/ZnO nanocomposite thin film on plasma treated polycrystalline Si wafers.

Neat PMMA film, due to the absence of atomic order, scattered X-rays in random directions and a broad signal without any high intensity peaks was obtained in the diffractogram which is characteristic of the amorphous phase. (Fig 3.6 a) However, PMMA/ZnO nanocomposite thin films with just 0.5 wt% ZnO mesocrystals displayed excellent crystallinity with very sharp and intense characteristic <100> peak of ZnO. (Fig 3.6 b) Other major peaks such as <101>, <002> were absent from the spectra thus confirming the preferential orientation of atomic planes in ZnO nanoclusters. A small peak with <110> orientation was also observed but with highly diminished intensity. The observed intensity of <100> peak was almost 20 times higher than that of <110> establishing the mechanism of Oriented Attachment process where the adjacent nanocrystals rotate and interact with neighboring crystals until their lattices align to minimize the surface energy of the resulting mesocrystal. The crystallite size, that is the size of a coherently diffracting domain and not necessarily the size of individual nanocrystals, was calculated using **Scherrer equation** [153] The calculated avg. value of D from XRD data was

55.08 nm which is in good agreement with the nanostructure size obtained from TEM images and also with the hydrodynamic radius calculated from DLS measurements. Although the individual nano-crystallite size ranges between 3-5 nm as analyzed from HRTEM images yet the $D_{avg}$ comes out to be the size of self-assembled nanoclusters. This observation further strengthens the Oriented attachment theory of crystal growth which states that the final structure typically diffracts as a single crystal, implying that the primary particles aligned during growth. [97][154] The d-spacing of crystal planes was calculated using **Bragg's equation.** [155] The average value of d-spacing came out to be 0.28 nm which strongly correlates with the d-spacing of <100> plane as measured from the SAED pattern (0.282 nm). This was attributed to the preferential orientation of self-assembled structures along a-axis implying that the maximum number of atoms were aligned along the surface contrary to the randomly aligned nanoparticles where <002> (c-axis orientation) is the relatively stronger intensity peak. [156]

### 3.4.3 Polydispersity, Surface potential and Colloidal stability

DLS measurements were undertaken on the colloidal nano ZnO suspension with ethanol as the dispersant medium. The solution was allowed to reach an equilibrium temperature of 25ºC before the runs started. Fig 3.7 (a) depicts the time evolution of correlation coefficient values which were used to compute the hydrodynamic radius. The y-intercept value which measures the signal/noise ratio was close to 1 indicating a high quality data with negligible noise. The decay rate of correlation coefficient was pretty rapid owing to the smaller size of the particles. Polydispersity index as indicated by the gradient of the decay curve represents a homogenous distribution of particles within a narrow size range. This was quantitatively confirmed by a low PI value of 0.23. The baseline smoothly decayed to zero without any contributions from bigger sized particles implying a unimodal distribution and absence of aggregates. This observation was consistent with the HRTEM and AFM images and also the zeta potential data which suggested strong repulsive forces between highly positive surfaces of modified ZnO nanostructures imparting them with excellent long-term colloidal stability

Fig 3.7 (b) shows the size distribution of particles as computed from the diffusion coefficient values. A narrow distribution was obtained, with an average Z value of 59.7 nm, implying uniformly sized particles as also indicated by the polydispersity index. The size measured from DLS experiments was slightly larger than the average particle size computed from HRTEM images. This could be attributed to the surface modification of ZnO nanostructures since DLS

measures the hydrodynamic radius which also includes a stable ionic boundary around the nanoparticle surface while HRTEM reveals the core particle size.

## Zeta Potential

Zeta potential becomes an extremely important physical quantity while formulating thin films and coatings based on complex hybrid systems with organic and inorganic phases having large contrast in polarity. [157] Nanoparticles having high surface energy tend to agglomerate in the polymer matrix resulting in translucent materials rather than optically transparent ones. Hence for optical applications, homogenous dispersion of ZnO nanostructures in PMMA is an essential requirement. [116] In our study, we modified the surface charges on ZnO nanoparticles by functionalizing with diethanolamine which is a cationic surfactant. Apart from mediating the self-assembly of ZnO nanoclusters, the adsorption of diethanolamine left the ZnO surface with excessive positive charges from the ionized amine moiety. These excessive positive ions attracted a large number of counter negative ions (Fig 3.9) thus increasing the potential at the surface of hydrodynamic shear i.e. the Zeta Potential. [157] Fig 3.8(a) depicts the Zeta potential of successfully functionalized ZnO nanostructures. A high positive value of 46.6 mV was obtained from the experiments that prevented flocculation and eventual phase separation in the colloidal system due to the electrical double layer repulsive forces being significantly stronger than the van der Waals attractive forces.

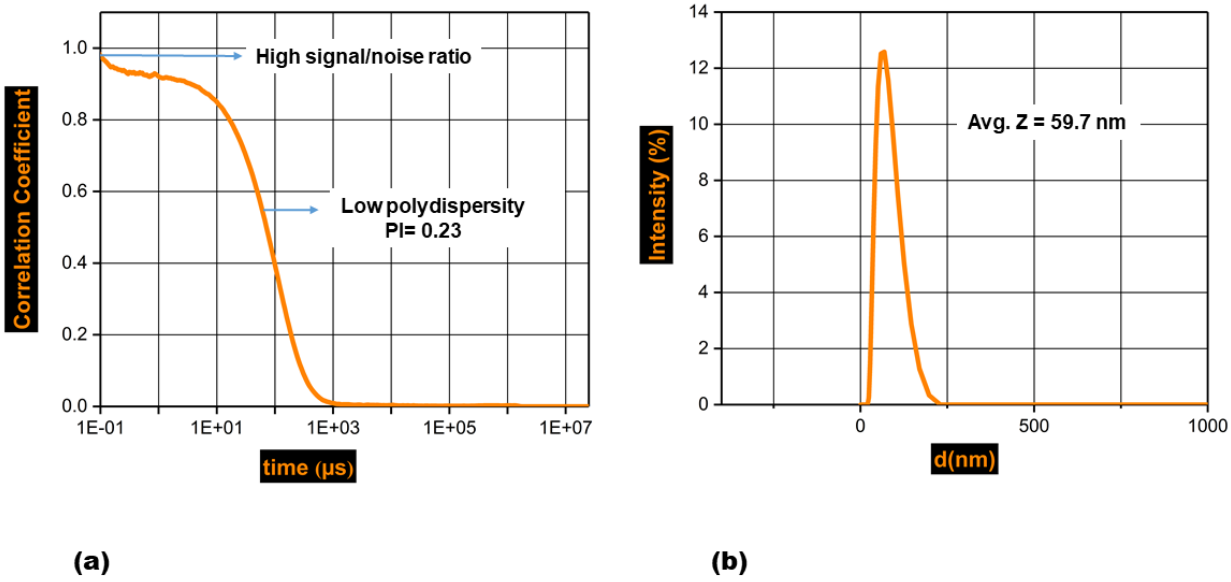


(a) (b)

Fig 3.7- DLS measurements on colloidal ZnO QD ethanol suspension: (a) Correlation coefficient decay curve vs. time and (b) Intensity-wise particle size (hydrodynamic radius) distribution

The long-term stability of the suspension was also quantified through DLS size measurements performed 24 weeks apart on the samples stored in ambient conditions. The obtained $Z_{avg}$ values had a remarkable correlation and the visible transparency remained unaffected. (Fig 3.8 (b))

It was established that high Zeta potential values rendered the ZnO nanostructures with exceptional long-term physico-chemical stability. Apart from inducing self-assembly and enhancing the surface charges, DEA also promoted chemical interactions between ZnO and PMMA phase thus resulting in a highly stable nanocomposite surface. The shift in the O-C=O peak binding energy and the presence of N-C=O peak in XPS survey confirmed the compatibility enhancement between polar ZnO nanostructures and non-polar PMMA matrix through the complexing process of DEA. This observation was consistent with AFM surface topography and FESEM images where we observed homogenously dispersed nanostructures and an overall smooth surface with low roughness values.

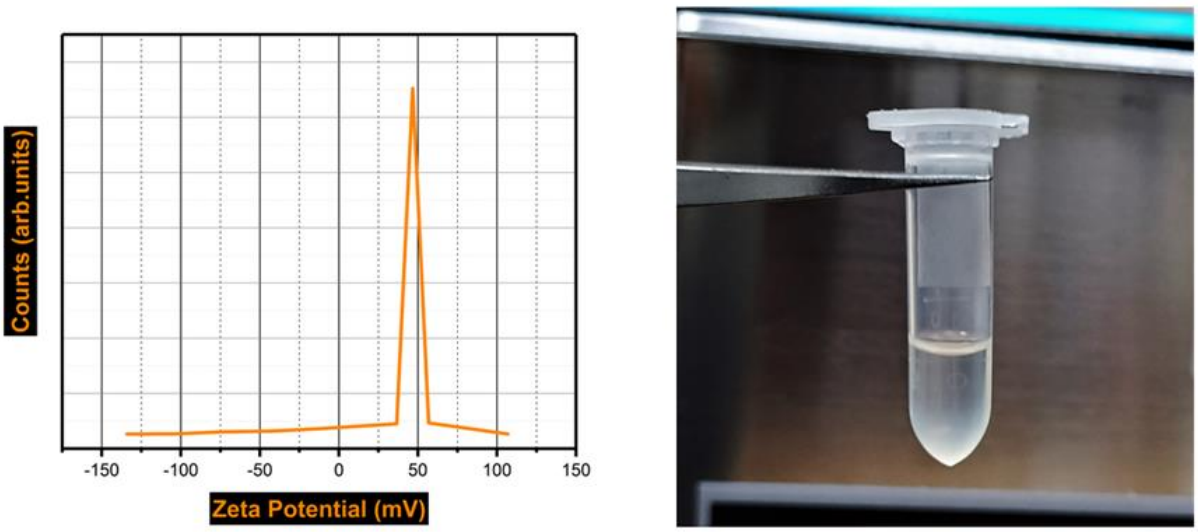


Fig 3.8- (a) Zeta potential of surface-engineered colloidal ZnO QD suspension with a high positive peak value of 46.6 mV and (b) Digital photograph of ZnO suspension with high transparency after 6 months of storage depicting excellent colloidal stability.

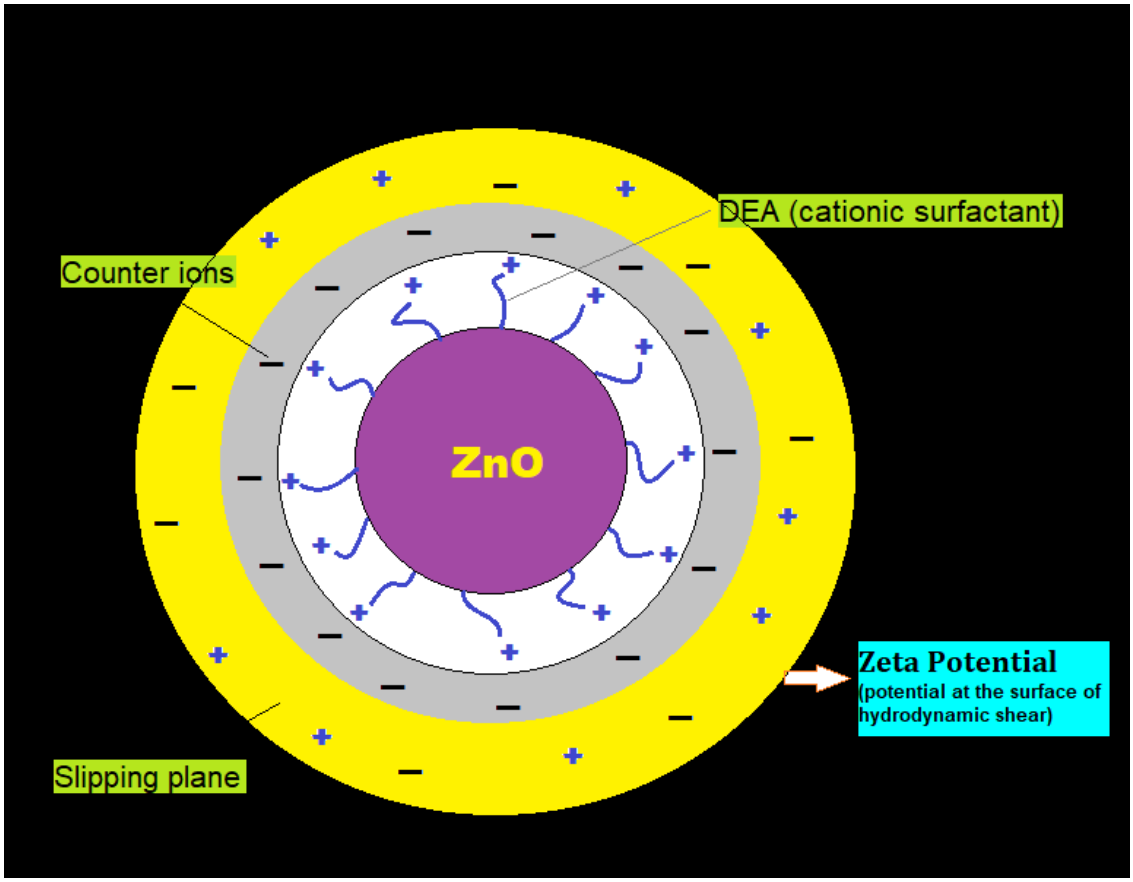


Fig 3.9- Schematic of ZnO surface charge modification by diethanolamine depicting the particle surface, stern layer and potential at the surface of slipping plane (Zeta potential)

### 3.4.4 Quantum Confinement in colloidal ZnO nanoclusters

UV-Visible absorbance data was used to calculate the average diameter of colloidal quantum dots constituting the nanocluster based on the method proposed by Meulenkamp. [158] It gives an experimental relationship between the average size of ZnO QD's and absorption shoulder ($\lambda_{1/2}$) :

$$1240/\lambda_{1/2} = 3.301 + 294.07/D^2 + 1.09/D \qquad (3.1)$$

where $\lambda_{1/2}$ (in nm) is the wavelength at which absorption is 50 % of the absorption shoulder and D (in Å) is the average diameter of particles. The size obtained using the above equation was 3.56 nm which is closely related to the HRTEM size distribution and also lies well within the quantum regime so as to observe size-dependent shift in optical parameters owing to the quantum confinement effect.

The first observation was the blue shift of absorption shoulder towards higher energy as evident from (Fig 3.10(a)). According to the literature, the excitonic peak for ZnO usually lies in the range of 350-370 nm for nanoparticles [159][160] and 380 nm for bulk while we obtained the value near 340 nm for green-emitting quantum dots. This was attributed to the restriction in the movement of electrons caused due to widening of the forbidden region between valence and conduction bands thus shifting the absorption spectrum towards higher energies.

Similarly, the band gap variation as compared to bulk ZnO also illustrated size dependent quantum effects. [161] The bandgap energy for colloidal ZnO QDs was calculated from the Tauc plot (Fig 3.10 (b)) using absorption spectrum data. [135] The absorption coefficient α is related to the band-gap energy $E_g$ by the relation-

$$(\alpha h\nu)^{\gamma} = A(h\nu - E_g) \qquad (3.2)$$

where ν is the photon frequency, A is a proportionality constant and γ denotes the nature of electronic transition having a value 2 for direct band gap transitions. We plotted $(\alpha h\nu)^2$ vs hν (Tauc plot) and extrapolated the linear region of curve to x-axis or α=0. The x-intercept value represented the band gap energy which was equal to 3.54 eV while the band gap values for bulk ZnO range between 3.3-3.4 eV. [162] A similar band gap shift was observed in the c-axis oriented self-assembled ZnO nanorods prepared by Tirado et al. using electrophoretic deposition technique.[163]

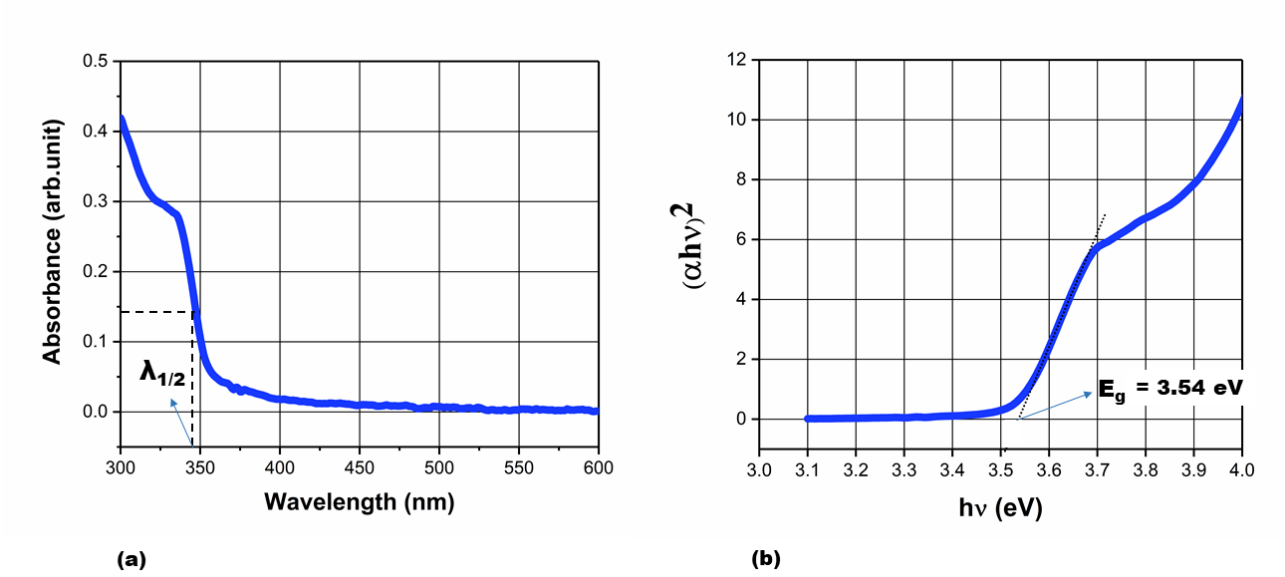


Fig 3.10- (a) UV-Vis absorbance data with $\lambda_{1/2}$ representation used in Meulenkamp method and (b) Tauc's plot depicting size-dependent blue shift in ZnO QD band gap.

The size-dependent shift in band gap energy is more prominent when the particle size reaches the limit of exciton Bohr radius ($r_b$) which is the distance between a pair of bound electron and hole. For a bulk semiconductor $r_b$ is expressed as-

$$r_b = \frac{h^2 \varepsilon}{4\pi^2 e^2}\left(\frac{1}{m_e} + \frac{1}{m_h}\right) \qquad (3.3)$$

where $m_e$ and $m_h$ are the effective masses of electrons and holes. ε, h and e are the optical dielectric constant, Planck's constant and the charge of an electron, respectively. The Bohr exciton radius for bulk ZnO is ~2.34 nm and the size calculated from absorption spectra was 3.56 nm. Within such close limits, the motion of the electrons and holes are confined spatially to the dimension of the QD which causes an increase in the excitonic transition energy and the observed blue shift in the QDs band-gap energy. [164]

The PL emission spectrum also illustrated size-dependent optical properties. The typical emission observed in ZnO quantum dots lies in the violet-blue region whereas we obtained a redshifted, strong green emission with a peak at 510 nm. This could be attributed to the size distribution of QDs in the 3-5 nm range while the blue emission is observed in much smaller particles with 1-2 nm diameters. [165] This suggests that by carefully controlling the synthesis

parameters such as surface capping time and molar ratio of ZnO precursor to diethanolamine, we can obtain nanostructures with strong, size-dependent photoluminescence that could be utilized in fabricating flexible, tunable light-emitting diodes and fluorescence-based sensors.

### 3.4.5 Interfacial defect induced PL emission

The visible emissions observed in PL emission spectra (Fig 3.11) of ZnO nanoclusters were purely attributed to the intrinsic defects and vacancies since no external doping was done in the synthesis process and XRD, EDAX peak data confirmed the absence of any unintended impurities. The dominant green emission peak at 510 nm was attributed to the deep level emission (DLE) associated with oxygen vacancies ($V_O$). Electron-hole recombination on singly charged oxygen vacancies ($V_{o+)}$ is the most widely accepted mechanism for green emission in ZnO quantum dots [166]–[168]. As calculated from the emission peak wavelength, the $V_o$ defect lies at an energy 2.44 eV below the conduction band. The concentration of oxygen vacancies on the surface was extremely high as evident from the narrow FWHM of the 510 nm peak which indicates that the ZnO nanoclusters possess excellent photocatalytic activity. The photocatalytic activity is boosted by the surface defects states and deteriorated by the core crystal structure defects that act as traps for charge carriers and decrease the number of free electrons and holes via recombination process. Due to the Oriented Attachment (OA) crystal growth, our ZnO nanoclusters had high crystallinity and minimum core crystal structure defects while the self-assembly and resulting porous mesocrystal morphology promoted the formation of excessive surface based Oxygen vacancies owing to the high aspect ratio. This morphology related interfacial defect concentration of the nanoclusters could remarkably enhance their photodegradation ability for removal of organic pollutants in water and also as high-performance sensors for toxic gases. The intensity of the green luminescence was extremely sharp indicating monodisperse particles which was already confirmed from the DLS and Zeta potential studies. A secondary emission peak at 610 nm in orange-red region was also observed. According to literature, the orange luminescence band can be attributed to the transition of electrons from conduction band to oxygen interstitials ($O_i$) located at 1.51 eV above the valance band. [169]

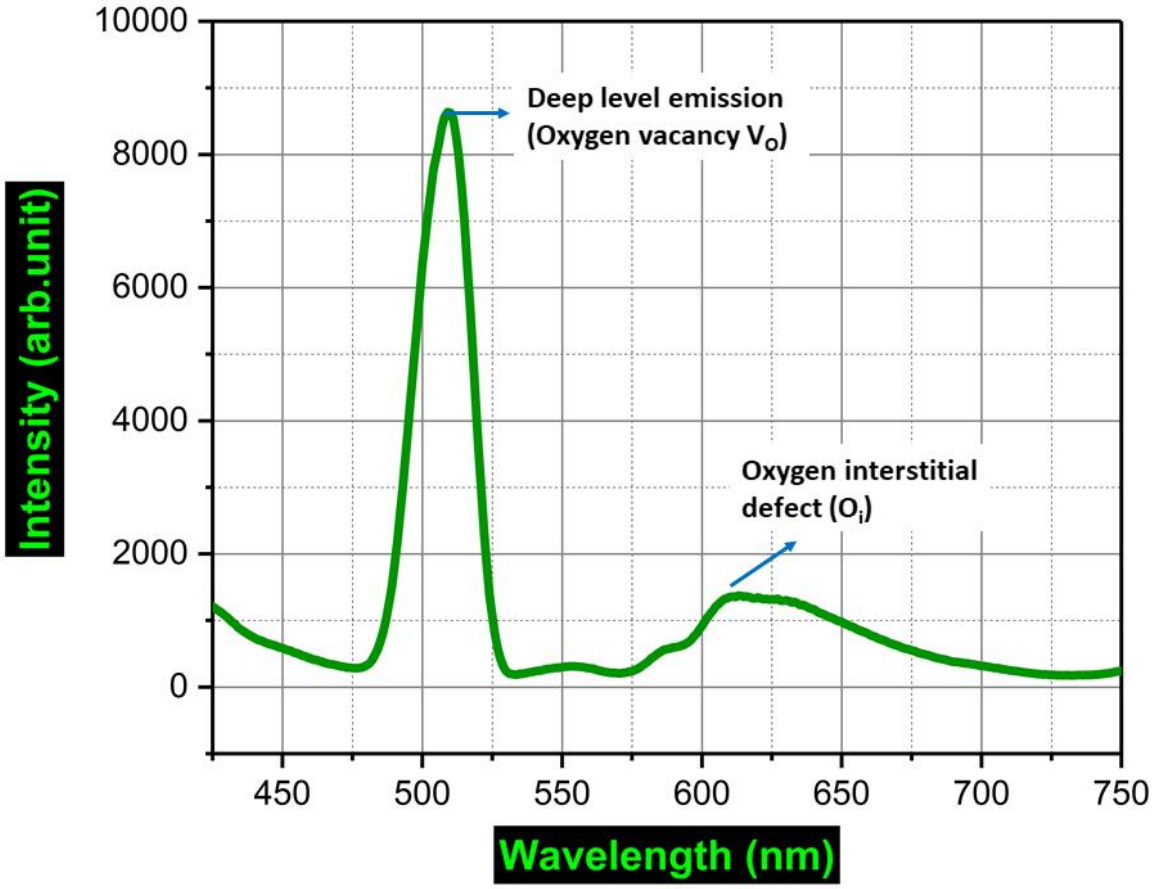


Fig 3.11- PL emission spectra of ZnO nanocluster depicting oxygen vacancy and oxygen interstitial surface defect induced green and orange emission bands respectively.

## 3.5 Conclusion

The study demonstrates biomimetic self-assembly of anisotropic semiconducting nanoclusters composed of ZnO Quantum Dots. The self-assembly obeyed non-classical crystallization mechanism where organic ligand conjugated nanocrystals grew into lattice aligned nanoclusters. Diethanolamine molecules incorporated themselves during the mesoscopic crystal growth and were part of the final crystal structure which is counterintuitive to the bulk ion by ion crystal growth. The oriented attachment (OA) process resulted in precisely aligned quantum dots possessing preferential orientation along <100> plane. Golic et al. [170]

synthesized self-assembled ZnO nanostructures by sol gel method without surface modification and did not observe any preferred lattice alignment thus establishing the significant role of DEA in Oriented Attachment mechanism achieved in our work. Owing to the unique structure and surface engineering, the colloids exhibited excellent long-term physico-chemical stability as evident from the DLS and Zeta potential studies. The final nanoclusters, even though 40-50 nm in size, retained the quantum characteristics of individual quantum dots and displayed size-dependent, tunable optical properties such as the wavelength of PL emission, blue shift of absorption shoulder and band gap energy which is a unique observation, characteristic of mesocrystal morphology and cannot be obtained in bulk nanostructures. Eita et al. [135] prepared spin-coated ZnO/PMMA thin films but did not observe quantum confinement effects in the band structure and obtained an $E_g$ value of 3.34 eV while the nanoclusters in our work displayed strong confinement with a blue-shift in band-gap energy to 3.54 eV. Surface morphology of mesocrystals implied a porous microstructure with highly enhanced effective surface area compared to bulk nanoparticles of similar size range. A large number of surface defects were induced in the nanoclusters owing to the unique crystallization mechanism which was experimentally confirmed by the sharp green PL emission peak with a narrow bandwidth. Diethanolamine moiety played a significant role in (a) Crystal growth and alignment, (b) Colloidal stability by altering the surface potential and (c) Promoting strong interfacial interactions between chemically opposite polar ZnO and non-polar PMMA phase.